MAGNETOMORPHIC OSCILLATIONS IN CADMIUM CYLINDERS

APPROVED:

J. O. Mackey
Major Professor

Tom J. Gray
Minor Professor

L. F. Bonnell, Jr.
Director of the Department of Physics

Robert B. Toulouse
Dean of the Graduate School

MAGNETOMORPHIC OSCILLATIONS IN CADMIUM CYLINDERS

THESIS

Presented to the Graduate Council of the
North Texas State University in Partial
Fulfillment of the Requirements

For the Degree of

MASTER OF SCIENCE

By

Ralph D. Hight, B.S.
Denton, Texas
August, 1969

TABLE OF CONTENTS

Page

LIST OF TABLES iv

LIST OF ILLUSTRATIONS v

Chapter

I. INTRODUCTION 1

II. APPARATUS AND EXPERIMENTAL PROCEDURE 4

Electrical Apparatus
Data Processing

III. THEORY 20

IV. EXPERIMENTAL RESULTS AND DISCUSSION 28

BIBLIOGRAPHY 42

LIST OF TABLES

Table		Page
I.	Theory Comparison	26
II.	Summary of Numerical Results	40

LIST OF ILLUSTRATIONS

Figure		Page
1.	X-Ray Tracing with Normal to Page	5
2.	Cylindrical Crystal	7
3.	Tool Design	8
4.	Polar Plot of Magnetoresistance	12
5.	Current Supply and Bell Hall Probe	13
6.	Data Taping System	15
7.	Sample Geometries	22
8.	Bulk Resistivities for Cerroseal Solder and Cadmium	29
9.	Oscillatory Component of the Magneto-resistivity	30
10.	Oscillatory Component of the Magneto-resistivity	31
11.	Oscillatory Component of the Hall Effect	33
12.	Oscillatory Component of the Hall Effect	34
13.	Period Plots.	37
14.	Peak to Peak Amplitude versus Magnetic Field.	38

CHAPTER I

INTRODUCTION

Boundary scattering of electrons in metallic conductors makes an appreciable contribution to the resistivity of the sample when the electron mean free path is comparable to a dimension of the sample. Sondheimer[1] has derived expressions for the electrical conductivity of thin films for a, or the magnetic field perpendicular to the plane of the sample, assuming a spherical Fermi surface and diffuse scattering. His expressions predicted oscillations in the Hall effect and the magneto-resistivity that are periodic in their magnetic field. Sondheimer's theory has since been extended to include ellipsoidal Fermi surfaces, Fermi surfaces of revolution about the normal to the plane of the sample,[2,3,4] and the effect of diffuse and specular scattering from the boundaries.[5]

The first observation of these oscillations was made by Babiskin and Siebenmann[6] in 1957, using a wire of sodium 80 microns in diameter at liquid helium temperatures. For lack of a theory for cylindrical geometry, Babiskin and Siebenmann used the wire diameter in place of the thin film thickness in Sondheimer's expressions for the period. The observed periods

agreed with those theoretically predicted to within about two percent. The observed oscillations showed a strong damping effect with increasing magnetic field.

In 1968, Mackey, Deering, and Sybert[7] treated the cylindrical-geometry case. Their expressions for the oscillatory resistivity components predicted an amplitude-damping effect as the magnetic field increased, and a different phase angle from that of Sondheimer's theory, with the wire diameter replacing the thin-film thickness in the expression for the period.

The work presented here is an experimental investigation of the effect of cylindrical geometry on electrical conductivity, in which single-crystal samples of cadmium at the temperature of liquid helium are used, with the diameter on the order of the electron mean free path.

CHAPTER BIBLIOGRAPHY

[1]E. H. Sondheimer, Phys. Rev. 80, 401-406, (1950).

[2]C. G. Grenier, K. R. Efferson, and R. M. Reynolds, Phys. Rev. 163, 406-420, (1966).

[3]V. L. Gurevich, Sov. Phys. JETP, 8, 464-470, (1959).

[4]H. J. Mackey, J. R. Sybert, and W. D. Deering, Phys. Rev. 172, 603, (1968).

[5]F. Fuchs, Proc. Cambridge Phil. Soc., 24, 100-108, (1938).

[6]J. Babiskin and P. H. Siebenmann, Phys. Rev., 107, 1249, (1957).

[7]H. J. Mackey, J. R. Sybert, and W. D. Deering, Phys. Rev. 176, 8561, (1968).

CHAPTER II

APPARATUS AND EXPERIMENTAL PROCEDURE

A single crystal ingot of 69-grade cadmium was obtained from Cominco American Incorporated, Spokane, Washington. The sample was oriented by taking Laue photographs of it after it was mounted on a two dimensional goniometer. The X-ray machine used was a Norelco X-ray generator equipped with a Polaroid XR-7 Cassette. The normal settings used were twenty-five kilovolts and twenty millamperes, with a twenty-minute time exposure. The exposure time could be reduced to ten minutes after chemically polishing the surface to be X-rayed with a one-normal nitric acid solution. Chemical polishing reduces the surface damage layer which results from the spark-cutting procedure.

Cadmium has a close-packed hexagonal crystalline structure. This structure is shown in Figure 1 by a Laue photograph taken of an oriented sample. The sample was oriented with the hexagonal axis parallel to the base of the goniometer. The goniometer with sample was then placed on a special mounting platform on a Servomet Spark Machine manufactured by Metals Research Ltd., Cambridge, England. The platform was oriented so that the cylinder to be cut had the hexagonal axis

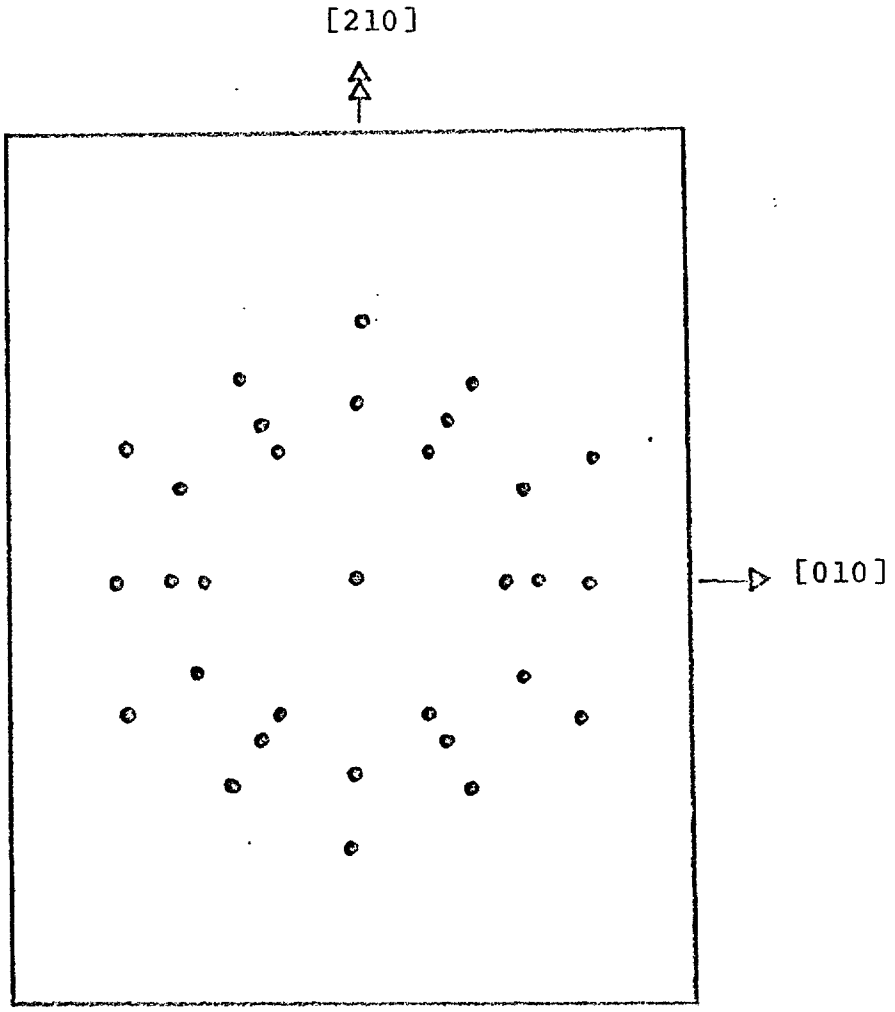

Figure 1--X-Ray Tracing with [001] Normal to Page

perpendicular and the binary axis parallel to the cylinder axis, as shown in Figure 2. The platform was then rotated by ninety degrees and the cylinder was separated from the main ingot by spark cutting, using a sheet of brass as the cutting tool. This procedure left the ingot oriented so that there would be no need to reorient the sample each time a cylinder was cut.

The tools designed to cut the cylinders are shown in Figure 3. The first tool was designed to minimize the strain on the crystal and to keep the cylinder from being further eroded by the spark-cutting process. Through reduction of the pressure on the inside of the tool, a flow of dielectric fluid was used to flush the cutting area and remove the sludge formed by the spark-cutting process. If the sludge is allowed to build up inside the tool, then spark eroding can occur. This effect was further reduced by having the inside diameter of the tool larger than the actual cutting hole. This precaution reduced tapering effects noted when the diameter was the same all along the tool. The cutting hole diameter was determined to be on the order of 200 microns larger than the diameter of the cylinder desired when operating the Servomet on range number six.

The cylinders produced had one percent taper of less, over a length of five to ten millimeters. The eccentricity of the cylinder was within one to two percent over the length

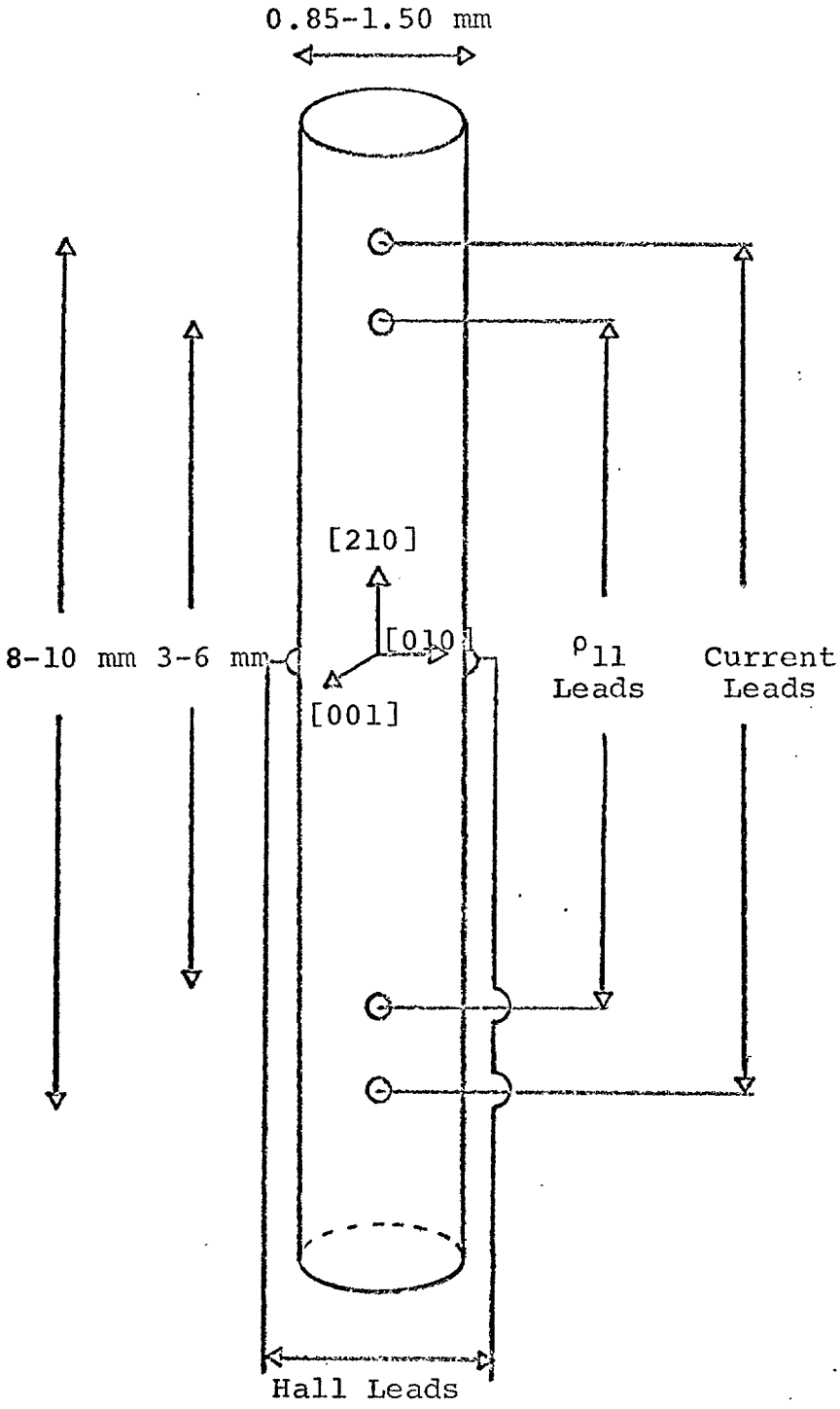

Figure 2--Cylindrical Crystal

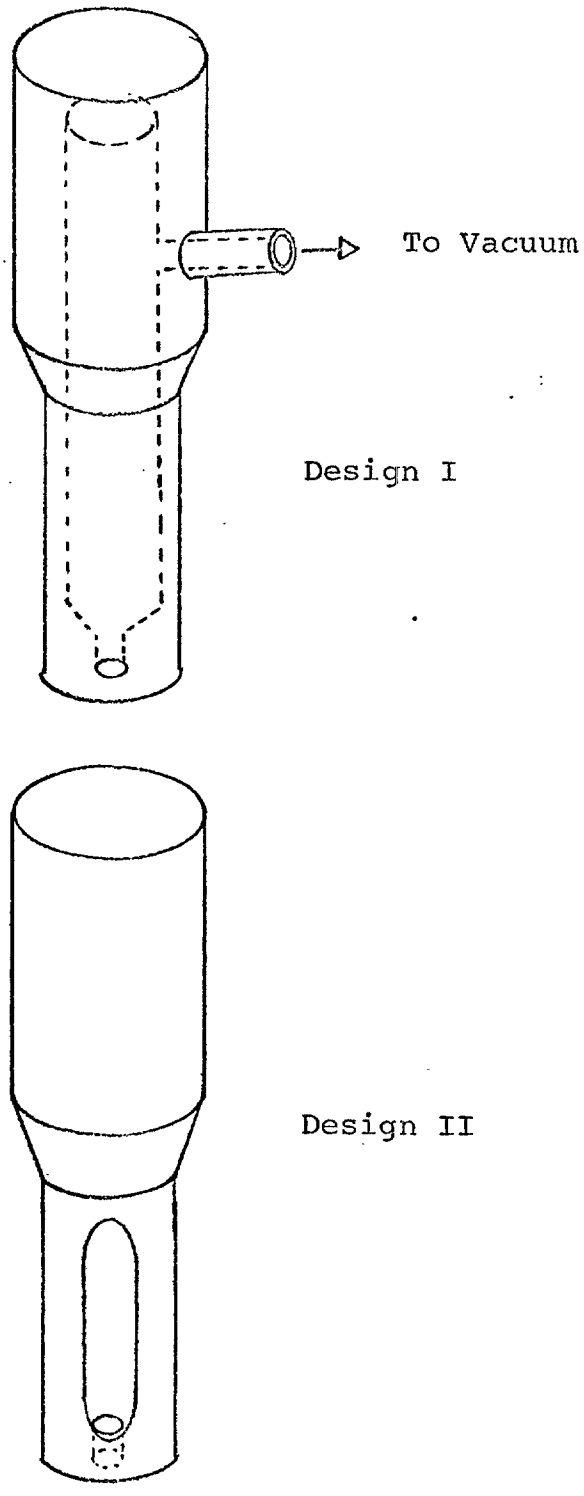

Figure 3--Tool Design

of the cylinder. The diameters ranged from 1.05 to 1.50 millimeters. This tool design worked extremely well for large diameter cylinders; however, it was found that for cylinders smaller than 1.00 millimeters, the cylinder would actually be struck during the cutting process. This striking was attributed to the small pressure gradient on the inside of the tool. A new tool was designed to eliminate this effect by machining windows in the sides of the tool to allow free flow of fluid without causing a pressure gradient along the length of the sample. These cadmium cylinders were on the order of 0.85 millimeters, with no bend, and the same order of taper and eccentricity as those produced according to the first design.

The crystal was treated with hot chromic acid to remove all oils and sludge from the surface. A light chemical polish with one-normal nitric acid solution removed some of the damaged layer and yielded a surface to which one could easily solder. It was found that polishing more than 100-200 microns off the diameter resulted in an oval cylinder, because the removal rate was faster along the hexagonal axis along the hexagonal axis than the bisectrix direction. Several cylinders were remounted on the X-ray machine and Laue photographs were taken. The small diameter resulted in the fact that a very small percentage of the total beam actually striking the crystal, thus necessitating a long exposure time. These photographs showed a hexagonal symmetry, confirming that the cylinders were still single crystals.

The crystal was then laid on a phenolic holder. Four tinned #34 wires were soldered to the cylinder with Sal-met flux and Cerroseal 35 solder composed of 50 percent indium and 50 percent tin. The wires are shown with respect to orientation in Figure 2. The current leads and magneto-resistivity leads were twisted together and soldered to separate pairs of wires that were shielded and attached to a current supply and a voltage-measuring system respectively. Hall probes were later attached across the diameter in an attempt to measure the Hall effect. For reasons discussed in the last chapter,another means of attaching leads was also used. Size 34 wires were spot-welded on the crystal by charging a 60 μf capacitor to 120 volts and then discharging it through the wire to the cylinder. The damaged area appeared to be of less extent than that of the solder blob.

The phenolic piece was mounted on a stainless steel holder designed to fit inside a Dewar and capable of making a vacuum seal. The design of the holder insured the fact that the axis of the cylinder was perpendicular to the magnetic field. The Dewar system used is described by Hathcox[1] and the procedure used to lower the temperature to liquid helium levels is given in detail by Miller[2]. The magnetic field was produced by a Pacific Electric Motor Company electromagnet, capable of fields from zero to plus or minus twenty-five kilogauss. Power for

the magnet was supplied by a Varian Associates Fieldial Power Supply capable of time-sweeping the magnetic field.

In order to orient the crystal with respect to the magnetic field, a plot of magnetoresistance versus the angle of the magnet at fixed magnetic field was made. The hexagonal axis is ninety degrees to a minimal point,as described by Fortmeyer[3]. A normal plot is shown in Figure 4. The minimum was found, and the magnet was then turned ninety degrees, so that the field was parallel to the hexagonal axis.

Electrical Apparatus

The current supply consisted of a twelve volt lead-acid battery in series with two variable resistors and an ammeter,as depicted in Figure 5. The current supply was electrically isolated from all other electrical equipment and was enclosed in an aluminum box to cut down on the possibility of pseudo-grounds which might be produced by the current supply. The leads from the box to the crystal were shielded,for the same reasons. The twelve-volt battery gave a constant preset current throughout the experiment.

The magneto and Hall resistivities were measured by recording the voltage drop across either pair of leads. By knowing the current I, the probe separation L and cross sectional area A of the sample, the resistivity ρ can then be calculated from

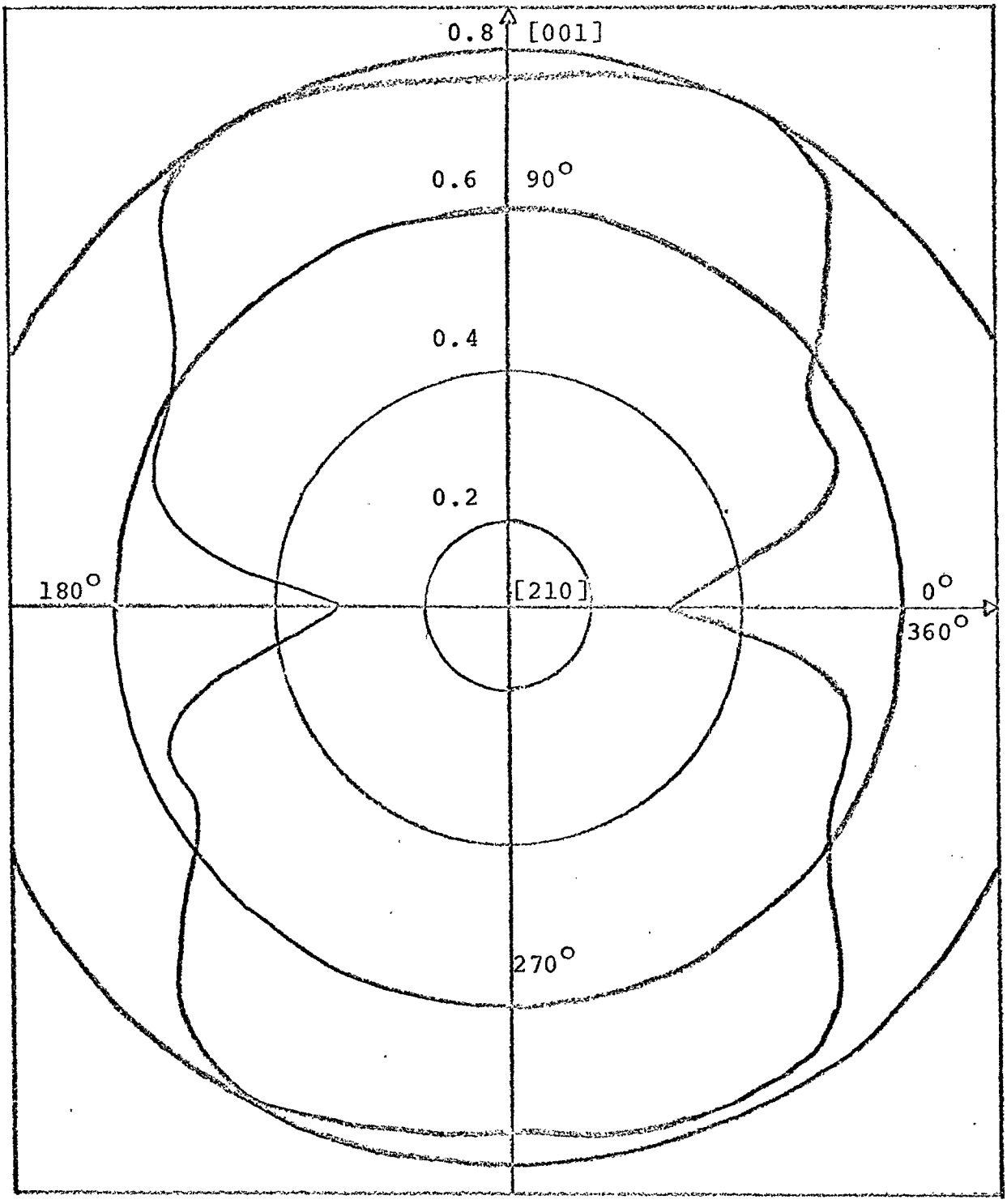

Figure 4--Polar Plot of Magnetoresistance

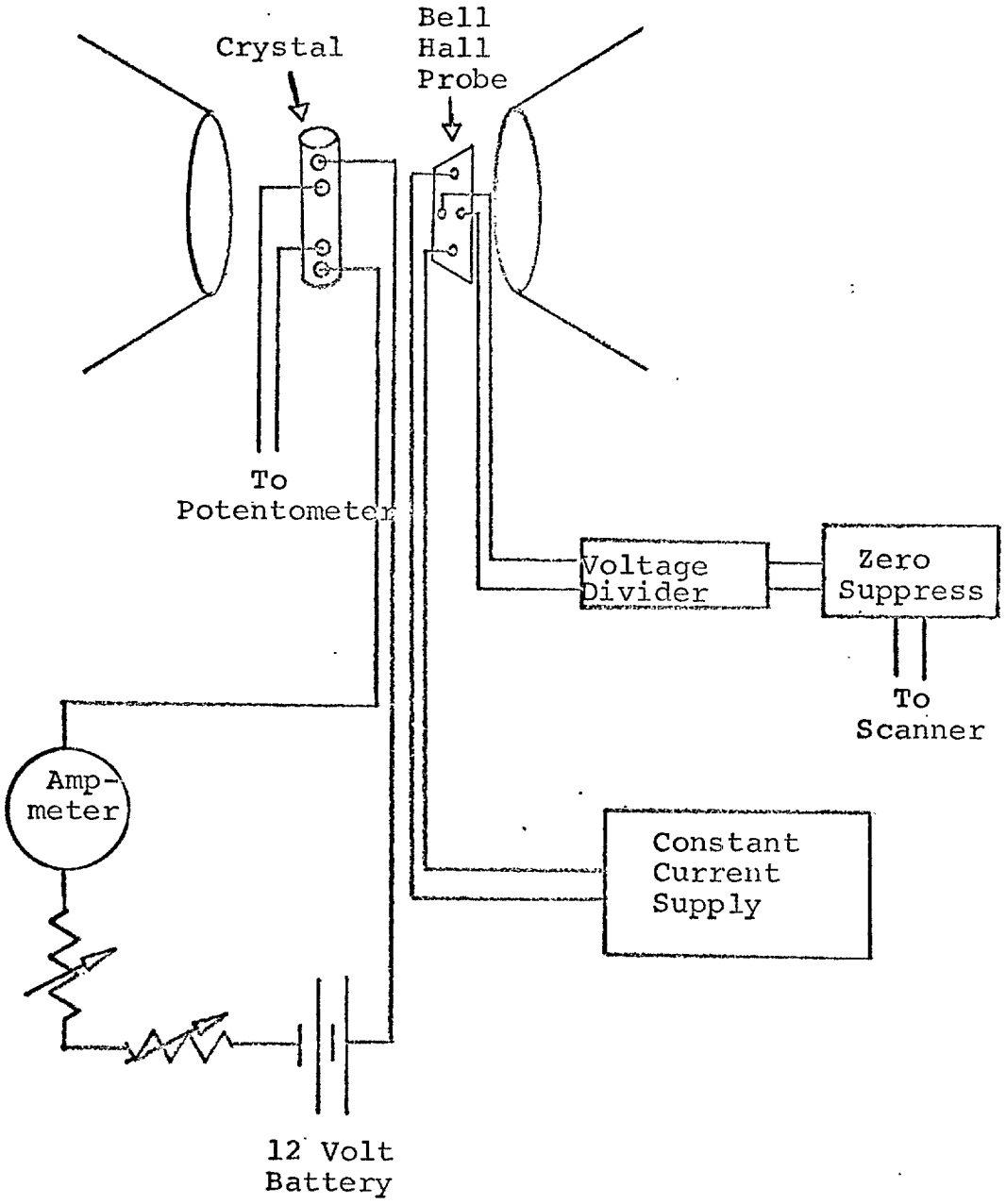

Figure 5--Current Supply and Bell Hall Probe

the voltage drop V from the equation

$$\rho = AV/LI \quad . \qquad (1)$$

The leads were attached to a six-dial Honeywell Potentiometer, the output of which was connected to a Keithley Model 148 Nanovoltmeter. The nanovoltmeter amplifies the input signal to drive a chart recorder. This voltage is placed in series with two voltage dividers. One voltage divider drives a Sargent Model SRG Chart recorder with the divider adjusted to full scale on the Keithley is full scale on the recorder. To calibrate the recorder, a known bias was added to the Keithley input by use of the potentiometer, and the resulting displacement on the recorder was noted. This system is diagramed in Figure 6.

In order to provide an accurate set of data that could be easily analyzed, a magnetic tape-recording system was assembled, as shown in Figure 6. A Kennedy Incremental 1400 magnetic tape recorder was employed in conjunction with a scanner developed by Systems Development, Inc., Dallas, Texas, and a Fairchild Digital Voltmeter, Model 7100 A.

The scanner consists of three channels. Each channel has both analog-coded and binary-coded decimal, referred to as BCD, inputs. Signals proportional to magnetic field and the resistivity of the crystal were connected to the analog inputs of channels one and two, respectively. All other inputs were

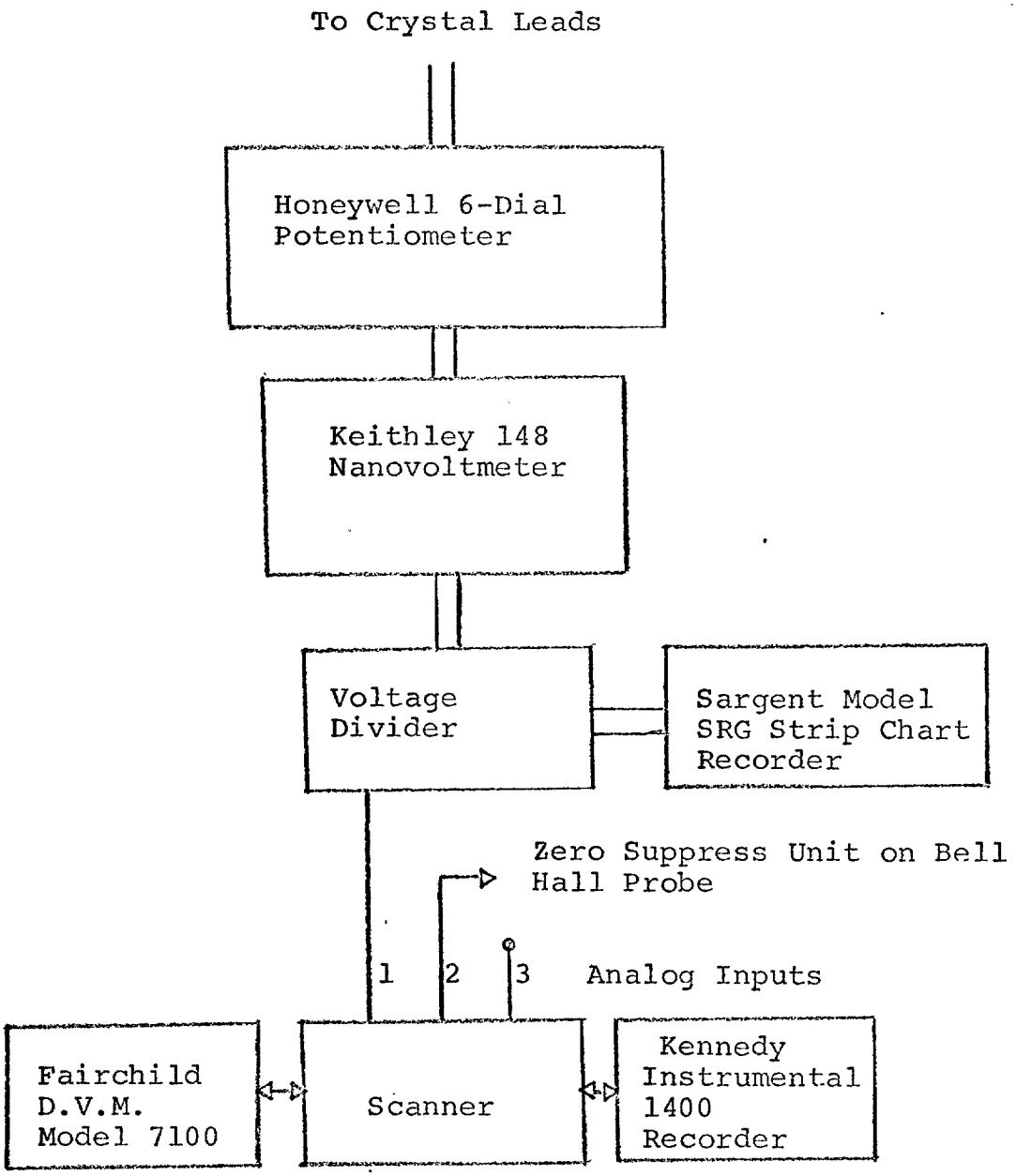

Figure 6--Data Taping System

by-passed. The scanner switches channel one and two alternately to the Fairchild. The BCD output of the Fairchild is routed back through the scanner to the recorder, to be placed on magnetic tape. The BCD format on the tape consists of a sign, five numbers, and a decimal point, in that order. Nine hundred and eighty digits per record, or 140 BCD numbers per record, were taken as a convenient record length. A counter on the scanner kept track of the number of records taken.

The voltage, from the second voltage divider in series with the Keithley output, was used as an input to channel two. The input in channel one for the magnetic field required the installation of a Bell Hall probe on a pole face of the magnet. This system, as shown in Figure 5, requires a constant current supply. The voltage output from the Hall leads in the probe was placed across a voltage divider and zero-suppress unit. The field was set at zero by use of a Bell 2400 Incremental Gaussmeter. Any residual voltage from the probe was eliminated by the zero-suppress unit. The magnetic field was then set at a known field and the voltage divider adjusted to read the fields in units of 10^{-5} volts. The system was accurate to within five gauss from zero to five kilogauss.

A typical run would consist of the following sets of records. The first record would be taken at zero field and current. The second record for calibration purposes would be taken with a known bias from the potentiometer. The third record would be at zero field but with current turned on. The field sweep would then be turned on and the system placed in automatic mode to record continuously the voltage changes. To obtain the required sensitivity, it was necessary to bias the signal to keep it within the range of the Keithley nanovoltmeter. The pause mode was used during biasing to stop the tape temporarily from recording. When a sweep was over, the last record was filled with nines to indicate the end of the sweep. A record at zero field with current still on was taken to determine whether there was any baseline drift. All required information, such as current values, bias voltages, crystal diamter, probe separation, and temperature,was recorded by hand in a notebook for later use in scaling the voltages to resistivities.

Data Processing

The data were compiled by converting the BCD numbers on the tape to actual voltage values on punch cards,by means of an IBM 1401 computer. These cards were then processed by four separate program routines on an IBM 1620 computer. The first program scaled the numbers to actual field and resistivity values.

The second program smoothed the data points and punched out values at equally spaced field values. The third program served a two-fold purpose. First, for magnetoresistance, the values for plus and minus field were averaged to eliminate any Hall effect present, since the Hall effect changes sign with the reversal of the magnetic field. Secondly, for the Hall resistance, the Hall resistivity values at minus field were subtracted from the plus field values and divided by two. The data now on punch cards were either all magnetoresistance or Hall effect, with no mixture of the two through misalignment of the probes. A curve was then fitted to the data by means of a quadratic of cubic equation, and the differences were printed out. The differences were graphed so that any oscillations might be observed. If any were present, then further computer analysis gave the period and phase angle of the oscillations.

CHAPTER BIBLIOGRAPHY

[1]Kyle L. Hathcox, unpublished master's thesis, Department of Physics, North Texas State University, (1968).

[2]Ronald E. Miller, unpublished master's thesis, Department of Physics, North Texas State University, (1966).

[3]Gary W. Fortmeyer, unpublished master's thesis, Department of Physics, North Texas State University, (1968).

CHAPTER III

THEORY

The isothermal electrical conductivity tensor, $\hat{\sigma}$, is defined by the equation

$$J = \hat{\sigma}E \quad , \tag{1}$$

where J is the current density and E is the applied electric field. To obtain theoretical expressions for the conductivity tensor, the Boltzmann transport equation is solved for the perturbed distribution function in the relaxation time approximation. In order to solve the Boltzmann equation, it is necessary to linearize the equation by neglecting deviations from Ohm's Law. The resulting equation is

$$v\cdot\nabla_x f_o - eE\cdot\nabla_p f_o - e/c\ vxH\cdot\nabla_p f + f_1/\tau = 0 \quad , \tag{2}$$

where f_o is the spherically symmetric equilibrium Fermi function, f_1 is the perturbation on f_o to produce f, H is the applied magnetic field, and τ is the isotropic relaxation time. The current density is defined by

$$J = -\frac{2e}{h^3} \int_p f v d^3p \quad , \tag{3}$$

where e is the electron charge, h is Planck's constant, f is the perturbed distribution function, v is the electron velocity, and d_p^3 is the differential momentum volume.

Sondheimer[1] has solved Eq. (2) for an infinite thin film with magnetic field perpendicular to the plane of the sample. Spherical Fermi surfaces and diffuse boundary scattering were assumed. The geometry is shown in Figure 7. Sondheimer's results were expressed in complex integral form with the bulk conductivity defined as

$$\sigma_B = nec(H_i - \hat{j}H)/(H^2 + H_i^2)$$

$$H_i = mc/e\tau \quad . \tag{4}$$

Grenier[2] expanded this integral by parts and found a good approximation for the high magnetic-field oscillatory components. These components are

$$\tilde{\sigma}_{11} = 3\ nec(H_o^3/H^4)e^{-a/\lambda}\cos(2\pi H/P_o) \tag{5}$$

$$\tilde{\sigma}_{12} = 3\ nec(H_o^3/H^4)e^{-a/\lambda}\cos(2\pi H/P_o + \pi/2) \quad , \tag{6}$$

where a is the film thickness, n is the electron density, p_F is the Fermi momentum, λ is the electron mean free path, H_o is equal to $p_F c/ea$, and P_o is equal to $2\pi H_o$.

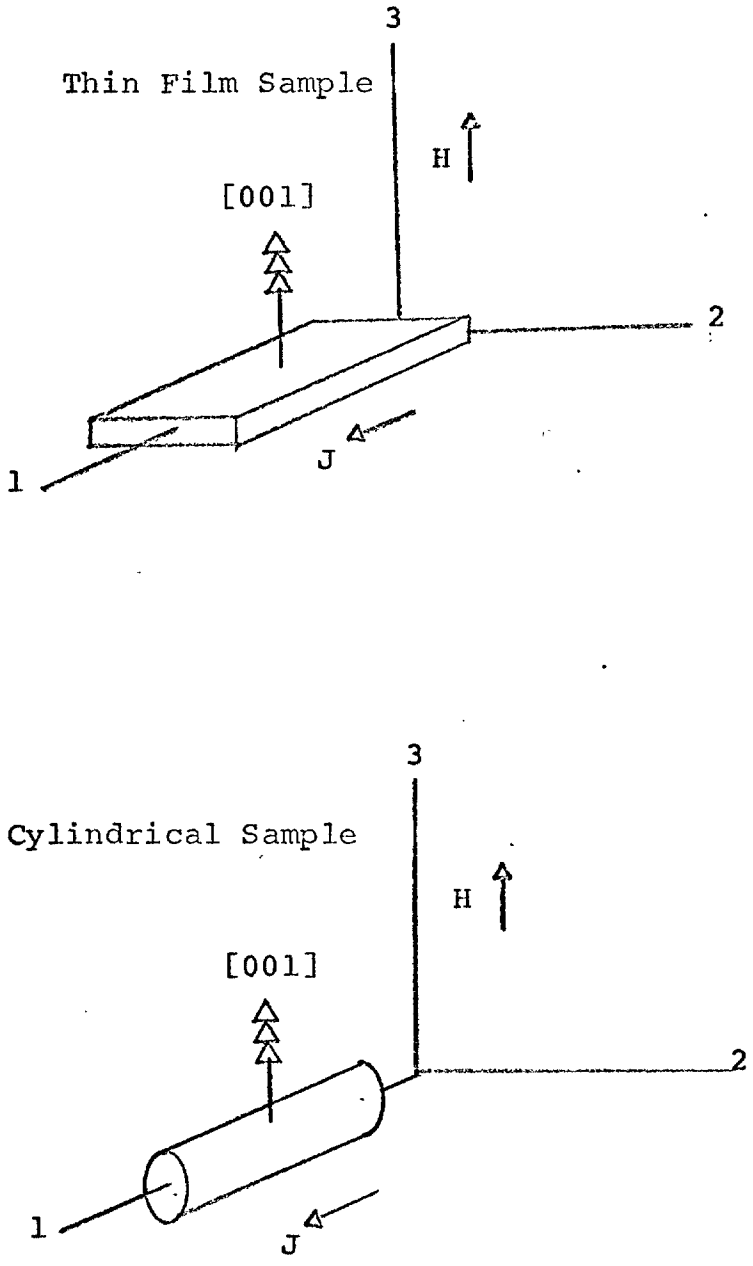

Figure 7--Sample Geometries

Gurevich[3] later showed that the period is proportional to the Gaussian radius of curvature of the Fermi surface at the point where the normal of the surface is parallel to the magnetic field, and to the cosine of the angle that the magnetic field makes with the normal to the plane of the sample. Gurevich also extended the theory to include arbitrary surfaces.

Mackey, Deering, and Sybert[4] have solved Eq. (2) for cylindrical geometry with magnetic field perpendicular to the cylinder axis, as shown in Figure 7. Their assumptions were the same as Sondheimer's, those being spherical Fermi surfaces and diffuse boundary scattering. The oscillatory terms they derived are

$$\tilde{\sigma}_{11} = 6(2/\pi)^{\frac{1}{2}} nec(H_o^{7/2}/H^{9/2}) e^{-2r/\lambda} \cos(2\pi H/P_o + \pi/4) \quad , \qquad (7)$$

$$\tilde{\sigma}_{12} = -6(2/\pi)^{\frac{1}{2}} nec(H_o^{7/2}/H^{9/2}) e^{-2r/\lambda} \cos(2\pi H/P_o - \pi/4) \quad , \qquad (8)$$

where r is the radius of the cylinder, and P_o is equal to $\pi p_F c/er$.

Most experimental data are in terms of resistivities instead of conductivities; therefore, considering the tensor relationship $\hat{\sigma} = \hat{\rho}^{-1}$, the following relationships can be shown:

$$\sigma_{11} = \frac{\rho_{11}}{(\rho_{11}^2 + \rho_{21}^2)} \quad ; \qquad (9)$$

$$\sigma_{12} = \frac{\rho_{21}}{(\rho_{11}^2 + \rho_{21}^2)} \quad . \tag{10}$$

In cadmium, for H along [001], ρ_{11} is quadratic in H and is much larger than ρ_{21} at high fields. These facts may be used to reduce Eqs. (9) and (10) to the following relations, valid at high fields:

$$\tilde{\rho}_{11} \simeq -H^4\tilde{\sigma}_{11} \quad ; \tag{11}$$

$$\tilde{\rho}_{21} \simeq H^4\tilde{\sigma}_{12} \quad . \tag{12}$$

Expressions for the resistivity may now be compared for the two geometrical cases. For the thin films, the resistivities are

$$\tilde{\rho}_{11} = \alpha\, e^{-a/\lambda}\cos(2\pi H/P_o) \tag{13}$$

$$\tilde{\rho}_{21} = \alpha\, e^{-a/\lambda}\cos(2\pi H/P_o + \pi/2) \quad , \tag{14}$$

where α is a multiplicative constant, and P_o is equal to $2\pi p_F c/ea$. The cylinder geometry solutions yield different expressions:

$$\tilde{\rho}_{11} = \beta\, e^{-2r/\lambda_H}H^{-\frac{1}{2}}\cos(2\pi H/P_o - 3\pi/4) \quad , \tag{15}$$

$$\tilde{\rho}_{21} = \beta\, e^{-2r/\lambda_H}H^{-\frac{1}{2}}\cos(2\pi H/P_o + 3\pi/4) \quad , \tag{16}$$

where β is a multiplicative constant, and P_o is equal to $\pi p_F c/er$. For comparison purposes, the difference in the two cases is listed in Table I.

TABLE I

THEORY COMPARISON

Sample Geometry	ρ_{ij}	Period	Phase Relative To Cosine	Damping
Thin Film	ρ_{11}	$P_o = \frac{2\pi p_F c}{ea}$	0	None
	ρ_{21}		$+\pi/2$	
Cylindrical Sample	ρ_{11}	$P_o = \frac{\pi p_F c}{er}$	$-3\pi/4$	$H^{-\frac{1}{2}}$
	ρ_{21}		$+3\pi/4$	

CHAPTER BIBLIOGRAPHY

[1]E. H. Sondheimer, Phys. Rev., 80, 401-406, (1950).

[2]C. G. Grenier, K. R. Efferson, and R. M. Reynolds, Phys. Rev., 163, 406-420, (1966).

[3]V. L. Gurevich, Sov. Phys. JETP, 8, 464-470, (1959).

[4]H. J. Mackey, J. R. Sybert, and W. D. Deering, Phys. Rev., 176, 856, (1968).

CHAPTER IV

EXPERIMENTAL RESULTS AND DISCUSSION

Initial measurements of the magnetoresistivity gave results as indicated in Figure 8. The presence of a very large hump was traced to the effects of the solder, used to attach the leads, going through a superconducting transition. Because of the small diameter of the cylindrical samples, the superconducting solder effectively shorted out an appreciable fraction of the length of the sample, resulting in a decreased potential. Figure 8 illustrates the magnetic behavior of Cerroseal 35 solder. At $4.2^{o}K$ the solder begins to go normal at 704 gauss, essentially saturating to a constant resistivity at approximately 1500 gauss, saturating by about 2700 gauss. Because, of this effect, leads were spot-welded on, the cadmium cylinders resulting in a normal quadratic magnetoresistance. Figures 9 and 10 indicate the oscillatory component ρ_{11}, measured in samples of diameter 1.05 mm and 0.90 mm respectively. It had been hoped that sufficiently accurage data could be obtained from magnetoresistance measurements alone, because of the difficulty of attaching Hall leads with solder points that were small compared to the cylinder diameters. For this reason, no Hall

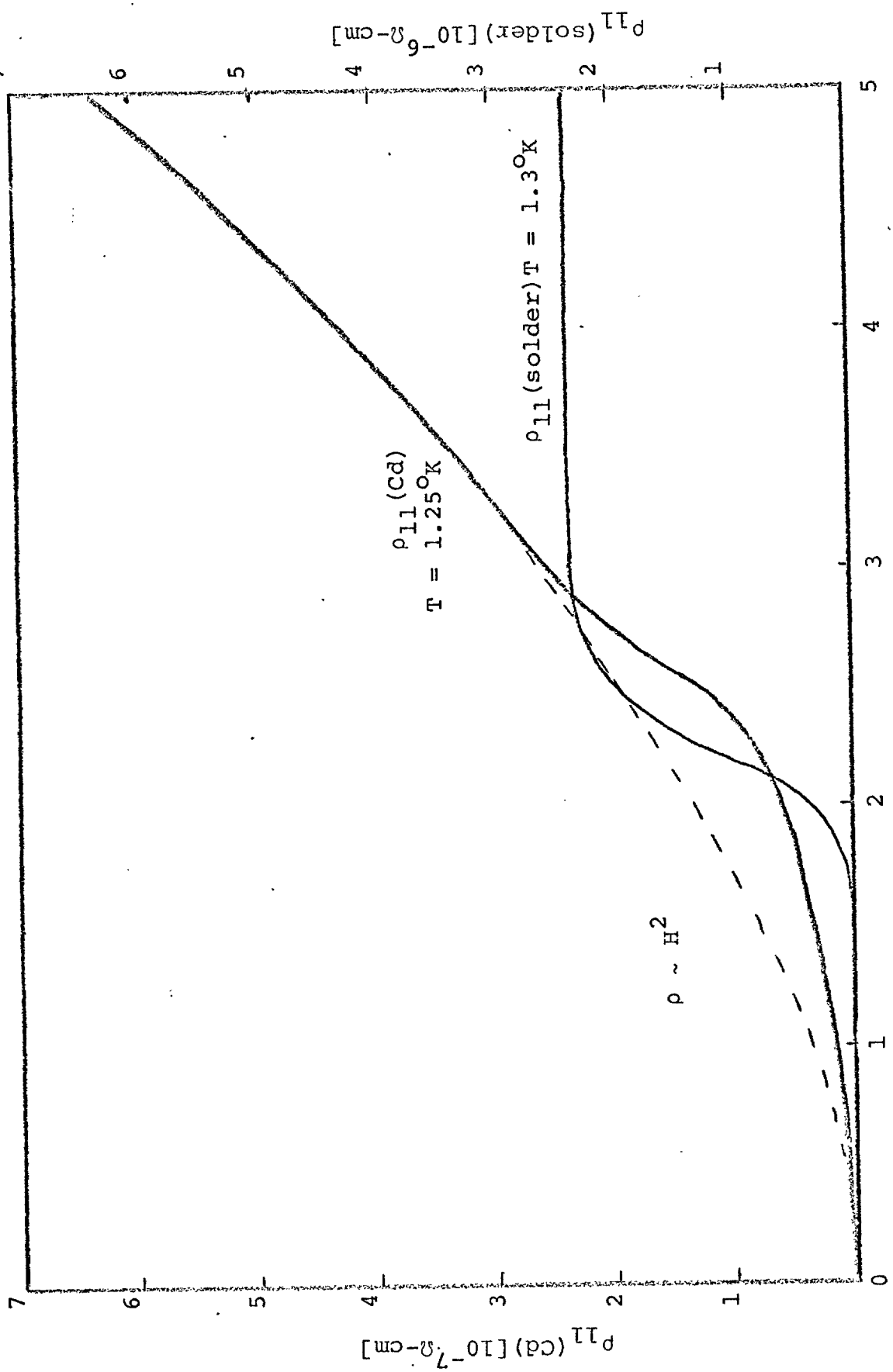

Figure 8--Bulk Resistivities for Cerroseal Solder and Cadmium

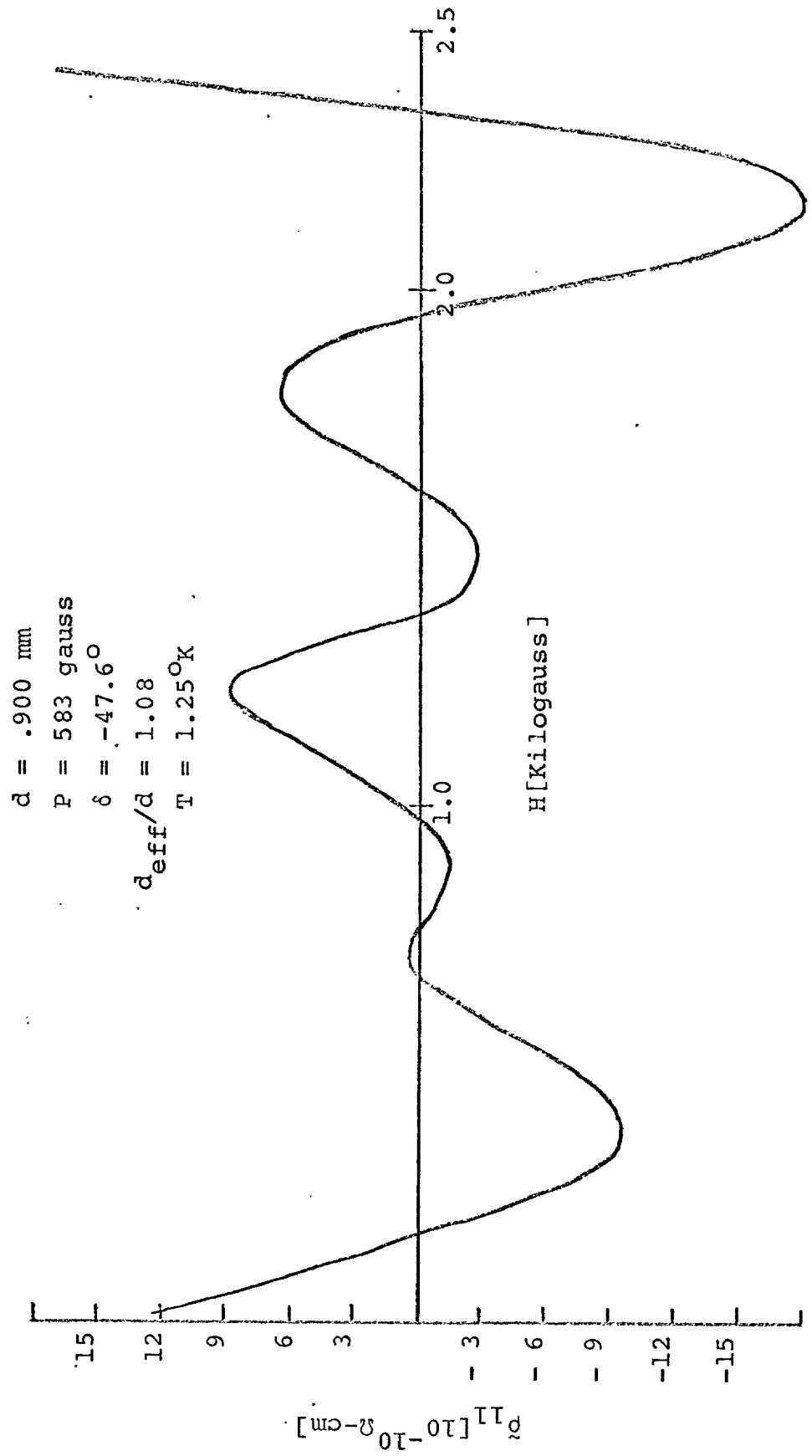

Figure 9--Oscillatory Component of the Magnetoresistivity

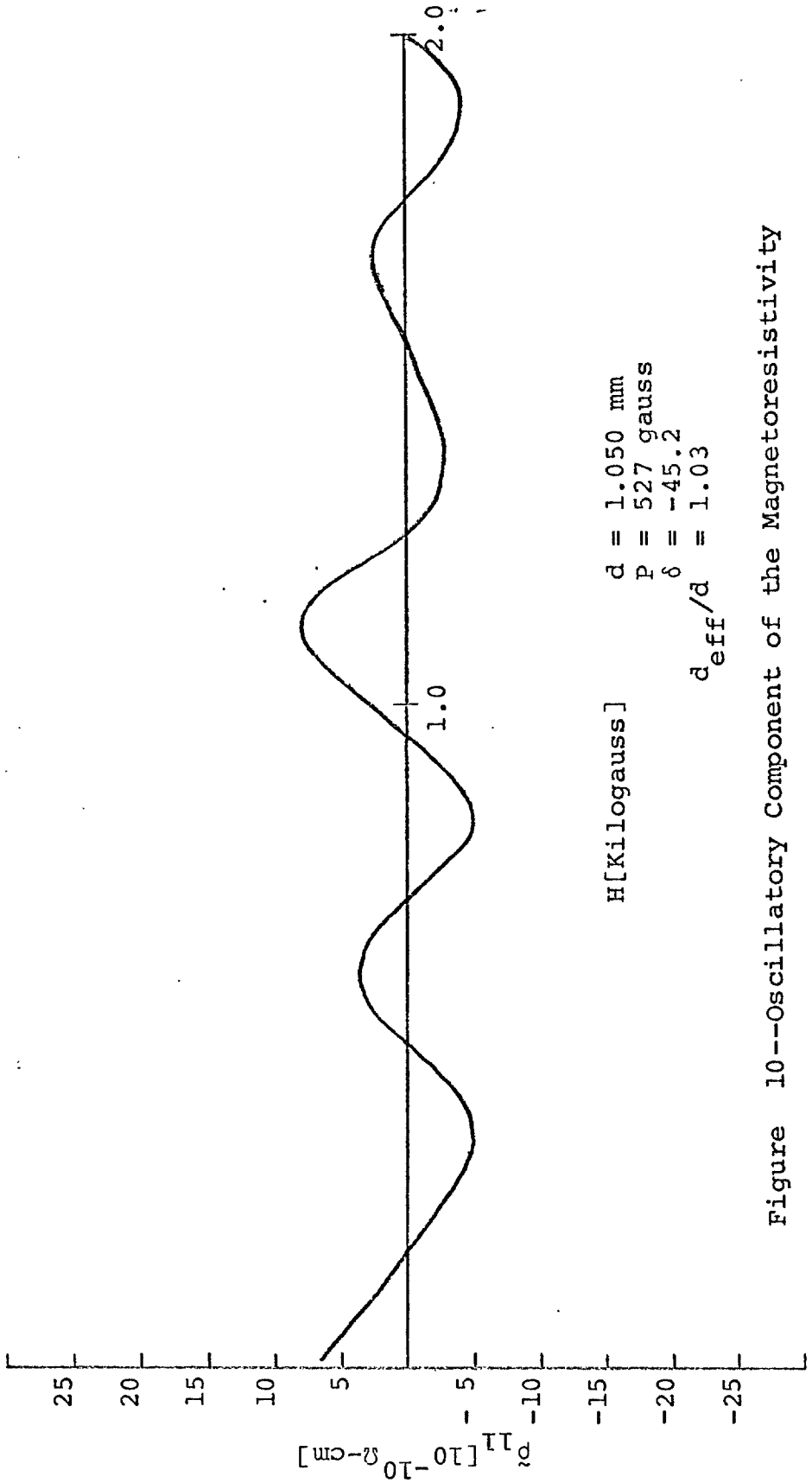

Figure 10--Oscillatory Component of the Magnetoresistivity

leads were attached to these two samples. The wander in the baseline indicated in these figures is due to the fact that the ratio $\tilde{\rho}_{11}/\rho_{11}$ is on the order of 0.03 at 1 kG and decreases quadratically (or faster) as the field is increased. Thus,even with extensive data smoothing by computer,it is possible to recover only marginally acceptable $\tilde{\rho}_{11}$ data from ρ_{11} data. At this point it was decided to attach Hall leads by spot welding. This was done on two separate samples, of diameters 1.26 mm and 0.85 mm. The resulting $\tilde{\rho}_{21}$ data are indicated in Figures 11 and 12,respectively. These data are much cleaner than the $\tilde{\rho}_{11}$ data of Figures 9 and 10,because of the fact that $\tilde{\rho}_{21}/\rho_{21}$ is much larger than $\tilde{\rho}_{11}/\rho_{11}$. Eqs. 7 and 8 in Chapter III predict that the $\tilde{\rho}_{ij}$ should exhibit maxima at magnetic field values given by

$$H = P_o(n - \delta/2\pi) \quad , \qquad (1)$$

where n = 0, 1, 2, ... with $\delta = -3\pi/4$ for $\tilde{\rho}_{11}$ and $\delta = +3\pi/4$ for $\tilde{\rho}_{21}$. Thus a plot of the values of magnetic field at which extrema occur against the integers (minima positions plotted at the half-integers) should yield a straight line whose slope is the period P_o and whose intercept is a measure at the phase δ. Figure 9 is such a plot for the four samples studied. Straight lines were fitted to the data by least squares. Table II gives a summary of the results obtained. It has been previously well established that the lens-shaped pocket of electrons

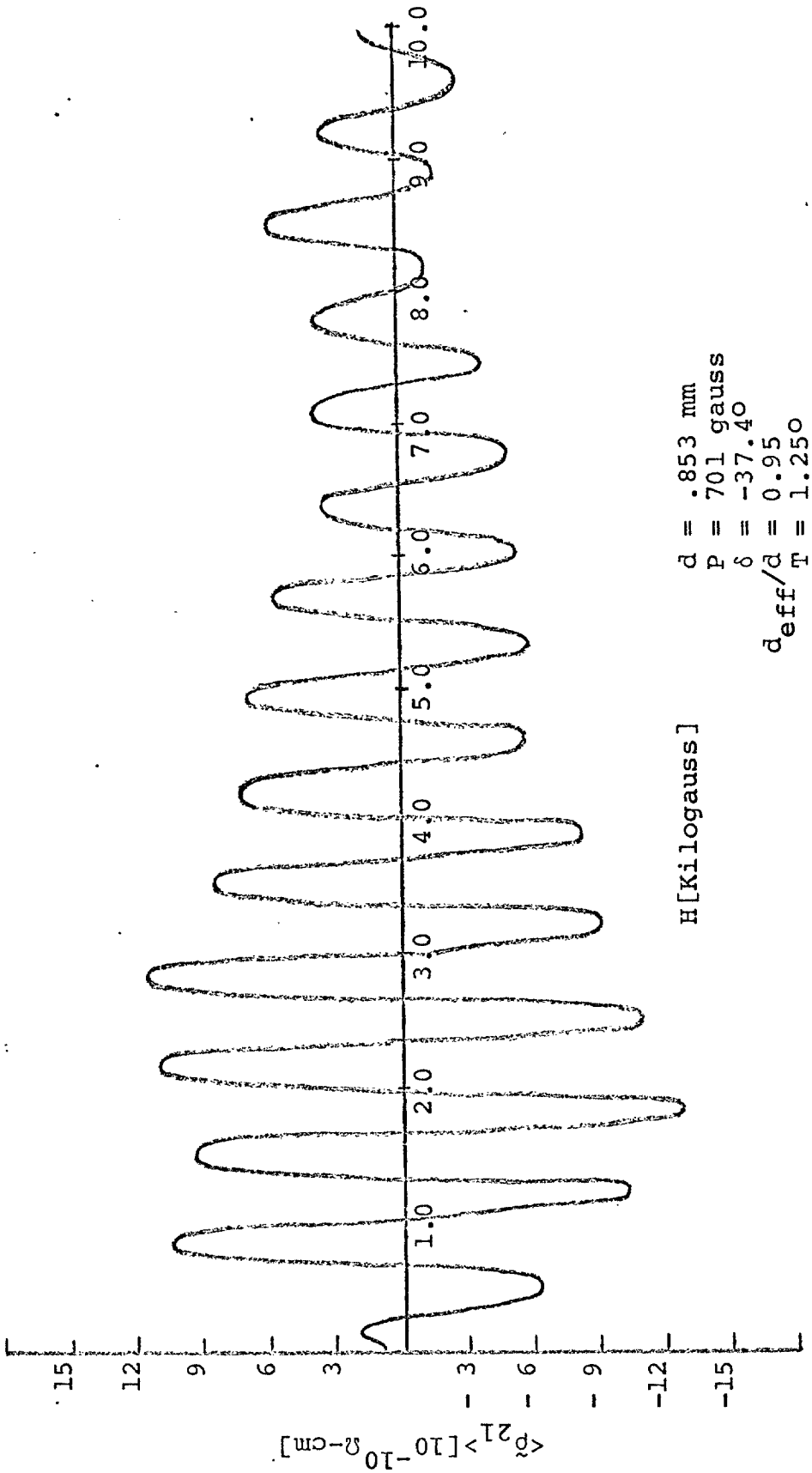

Figure 11--Oscillatory Component of the Hall Effect

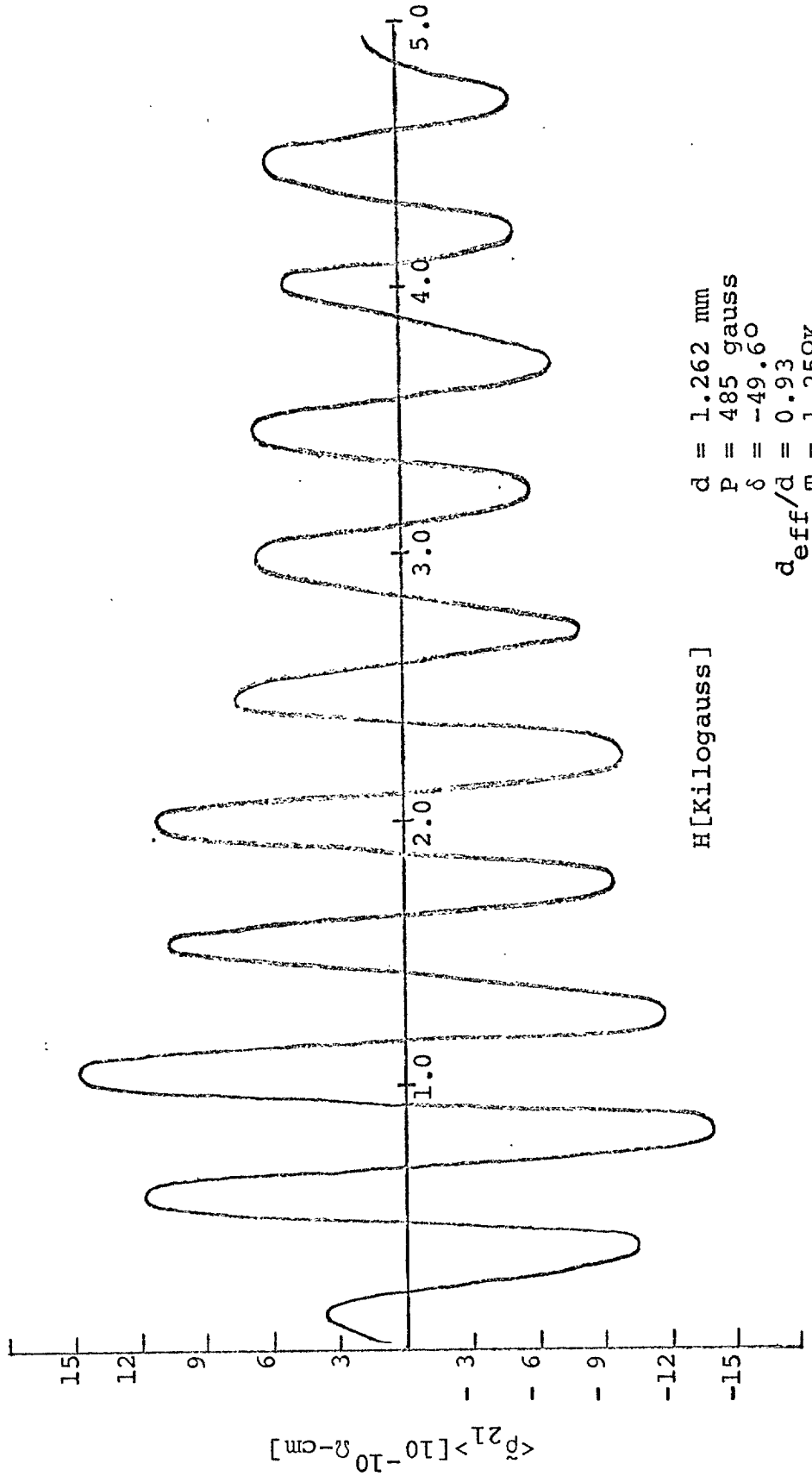

Figure 12--Oscillatory Component of the Hall Effect

in the third zone is responsible for the major Sondheimer oscillations in cadmium. Grenier[1] et al. have also observed a contribution due to the "hole arms" in the second zones, producing a period of approximately 25 percent and an amplitude of about ten percent of the electron oscillations. Although the theory for cylindrical geometry has assumed a spherical Fermi surface, one may reasonably assume that the Fermi momentum p_F which occurs in the period may be replaced by g, the Gaussian radius of curvature of the apex of the lens surface in accordance with the results of Gurevich. One then obtains the expression

$$d = 569/P_o \text{ mm} \quad , \qquad (2)$$

relating the cylinder diameter d to the period P_o of the lens oscillations, when P_o is expressed in gauss. One may insert the measured period into Eq. (2) to calculate d_{eff}, the effective diameter. Table II contains the entry d_{eff}/d, where d is the measured diameter. This quantity should equal one for exact agreement with theory. It is seen that the error ranges from -7 percent to +8 percent. It is most probable that the period is actually determined by the ratio g/d and that the noted error is purely experimental. It should be pointed out, however, that the oscillatory expressions given in Eqs. (7) and (8) of Chapter III are obtained as asymptotic functions valid

at high field. Thus inclusion of all maxima and minima in the plots of Figure 13 is not strictly correct. Eqs. (7) and (8) in Chapter III imply that $\delta = -135^{o}$ for $\tilde{\rho}_{11}$ and $\delta = +135^{o}$ for $\tilde{\rho}_{21}$. As seen in Table II, δ appears to be approximately -45^{o} for both $\tilde{\rho}_{11}$ and $\tilde{\rho}_{21}$. As noted above, the phase is not determined. Eqs. (7) and (8) in Chapter III imply that $\tilde{\rho}_{11}$ and $\tilde{\rho}_{21}$ should damp as $H^{-\frac{1}{2}}$, as the magnetic field is increased. Figure 14 is a plot of the peak amplitudes observed on the two $\tilde{\rho}_{21}$ samples. The amplitude grows at first and then decreases. Ignoring the initial rise, a logarithmic least-square fit was made, to $y = Ax^{m}$, to estimate the damping exponent m. The exponent was found to be m = -1.04 for the 0.85 sample, and m = -0.595 for the 1.26 mm sample. Although the spark-cut samples were treated with a light nitric-acid polish, there probably reamins a shallow distorted region at the sample surface. This is consistent with the d_{eff}/d less than one values found for the clean $\tilde{\rho}_{21}$ data. Such a distortion layer would increase the damping rate and would be more significant in comparison with the diameter in smaller samples. Thus, although not demonstrated to be 0.5, it is likely that the true absolute value of m is less than 0.6.

In summary the following conclusions may be drawn from this investigation:

(1) It is possible to produce submillimeter cylindrical samples by spark-paning without significant decrease

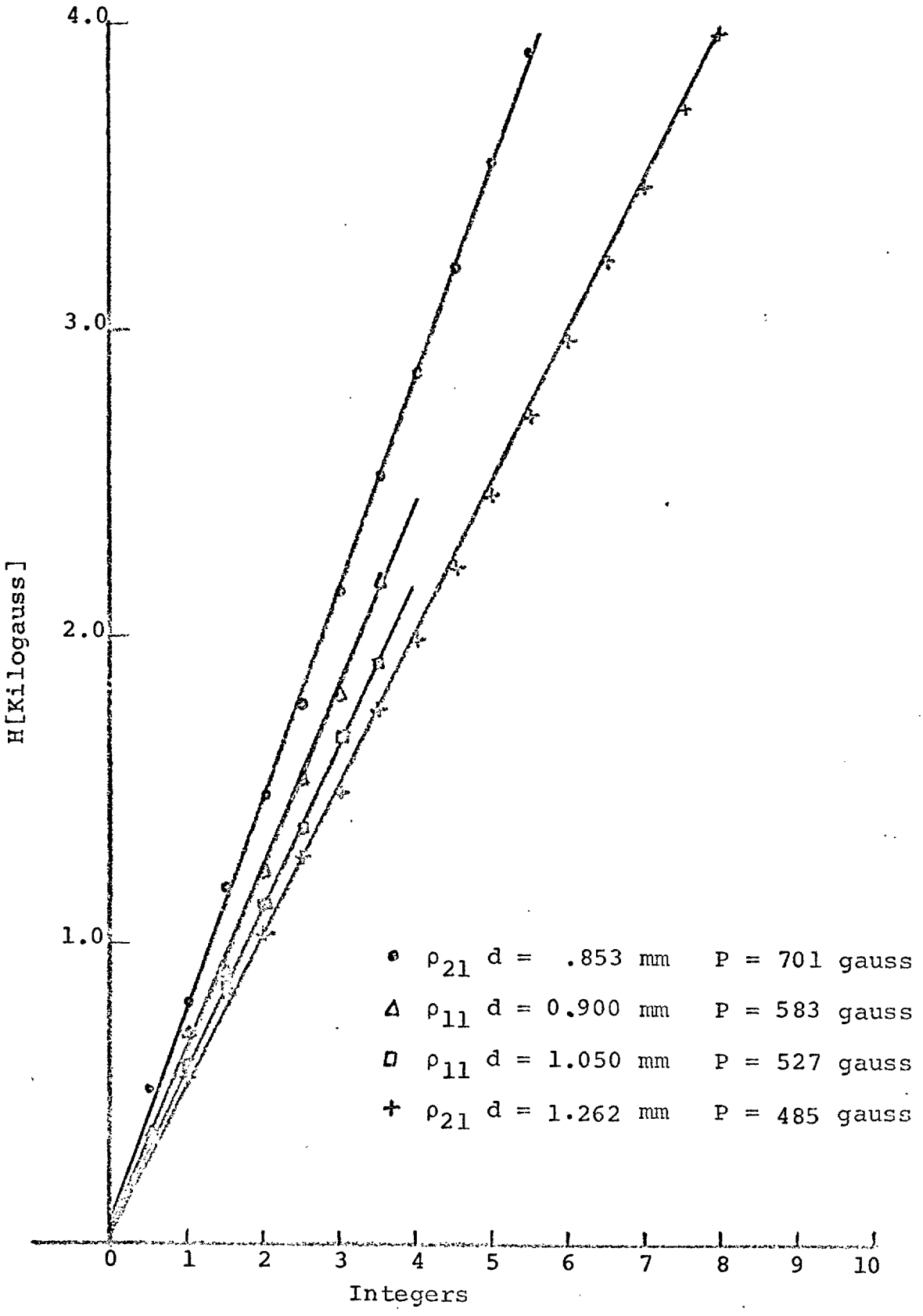

Figure 13--Period Plots

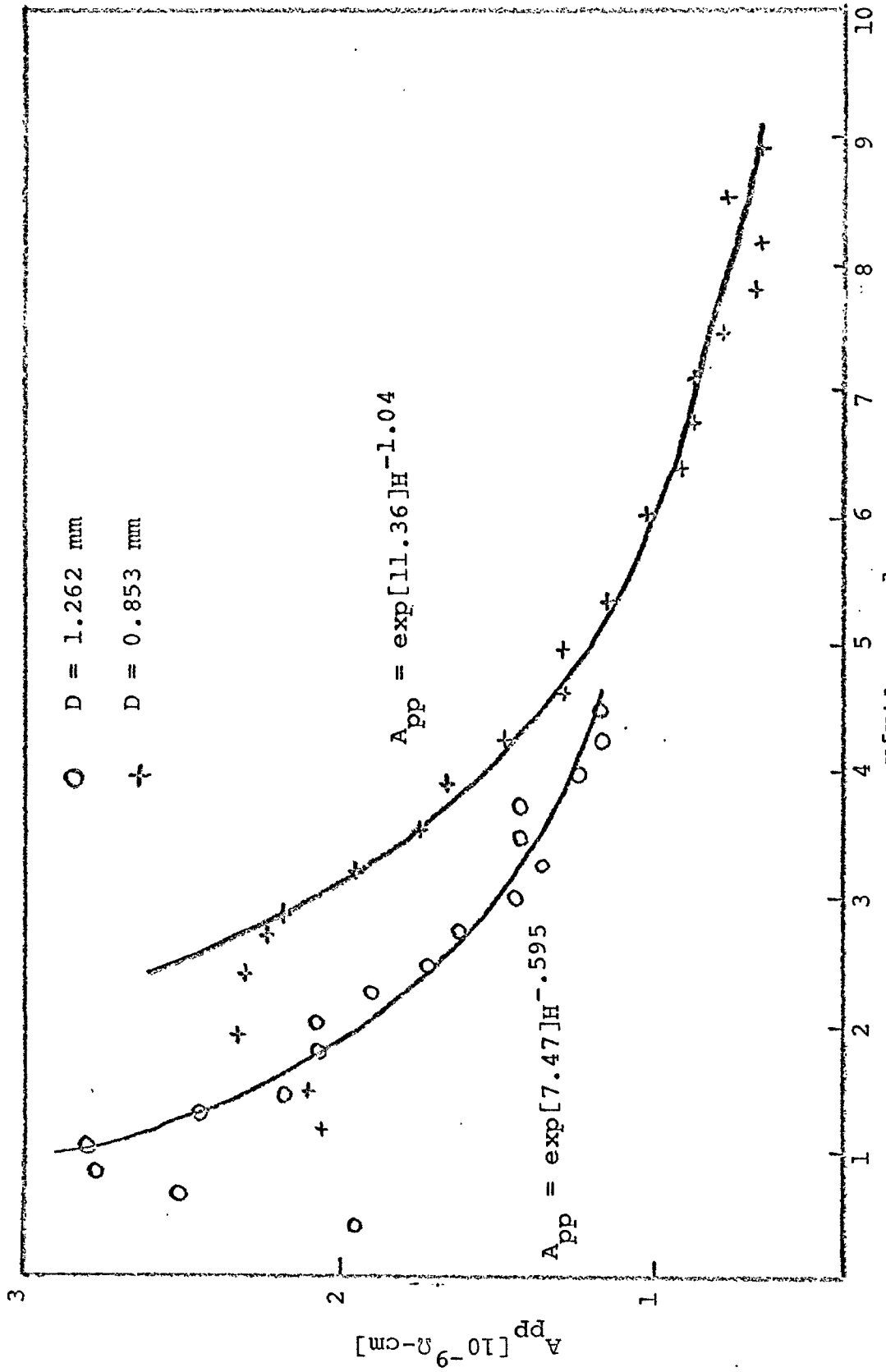

Figure 14--Peak to Peak Amplitude Versus Magnetic Field

in the bulk mean-free-path. This is evidenced by the fact that the oscillations can be observed in such samples, and that their amplitude is approximately the same as in films of equivalent thickness.

(2) The period is determined by the ratio g/d,in good agreement with theory.

(3) The amplitude damps more rapidly than predicted by theory,but the damping rate appears to approach the theoretical value $H^{-\frac{1}{2}}$ in samples where the depth of damage due to spark-planing is a small percent of the cylinder diameter.

(4) The theoretically predicted phases cannot be confirmed by the available data. The oscillations are not strictly sinusoidal in the field range studied, and therefore the phases obtained are in question.

TABLE II

SUMMARY OF NUMERICAL RESULTS

d mm	$\tilde{\rho}_{ij}$	P_o Gauss	δ Degrees	d_{eff}/d
1.05	$\tilde{\rho}_{11}$	527	-45.2	1.03
0.90	$\tilde{\rho}_{11}$	583	-47.6	1.08
1.26	$\tilde{\rho}_{21}$	485	-49.6	0.93
0.85	$\tilde{\rho}_{21}$	701	-37.4	0.95

CHAPTER BIBLIOGRAPHY

[1]C. G. Grenier, K. R. Efferson, and R. M. Reynolds, Phys. Rev. 163, 406-420, (1966).

BIBLIOGRAPHY

Articles

J. Babiskin, and P. H. Siebenmann, Phys. Rev., 107, 1249, (1957).

F. Fuchs, Proc. Cambridge Phil. Soc., 24, 100-108, (1938).

C. G. Grenier, K. R. Efferson, and R. M. Reynolds, Phys. Rev., 163, 406-420, (1966).

V. L. Gurevich, Sov. Phys. JETP, 8, 464-470, (1959).

H. J. Mackey, J. R. Sybert, and W. D. Deering, Phys. Rev., 172, 603, (1968).

H. J. Mackey, J. R. Sybert, and W. D. Deering, Phys. Rev., 176, 8561, (1968).

E. H. Sondheimer, Phys. Rev., 80, 401-406, (1950).

Unpublished Materials

Gary W. Fortmeyer, unpublished master's thesis, Department of Physics, North Texas State University, (1968).

Kyle L. Hathcox, unpublished master's thesis, Department of Physics, North Texas State University, (1968).

Ronald E. Miller, unpublished master's thesis, Department of Physics, North Texas State University, (1966).